Energy materials

CrossMark

Microwave-assisted exfoliation strategy to boost the energy storage capability of carbon fibers for supercapacitors

Junxian Zhang[1], Xin Zhao[1,*], Mengyao Yao[1], Wenjun Tan[1], Jie Dong[1], and Qinghua Zhang[1,*]

[1] State Key Laboratory for Modification of Chemical Fibers and Polymer Materials, College of Materials Science and Engineering, Donghua University, Shanghai 201620, China

ABSTRACT

Carbon fibers, with reduced oxidized graphite layers on the surface obtained using a facile method, were developed as one-dimensional electrodes. The oxidized layers directly formed from the surface of the carbon fibers had a strong interconnectivity with the fiber core, and their conductivity was apparently improved after reduction by hydrazine hydrate. With an abundance of oxygen functional groups induced by oxidation, the one-dimensional electrodes showed a specific capacitance of 213.3 F g^{-1} at a current density of 0.1 A g^{-1}, which was forty times more than that of the original carbon fibers when tested in a three-electrode configuration. The innately stability in aqueous solutions and the graphite layers from the carbon fibers themselves made the electrodes based on the carbon fibers endowed optimal cycling ability without a decline in specific capacitance after 10000 cycles. The device made of CF-R had a good energy density performance. This strategy provided a facile way to obtain a one-dimensional electrode with a high specific capacitance and good durability for energy storage systems.

Introduction

With the continuous increase in the electrical device usage, energy storage systems have attracted considerable attention from several researchers and companies all over the world. In particular, supercapacitors have been regarded as one of the most promising energy storage devices because of their higher power density and greater endurance than those of secondary batteries, while they can maintain nearly the same energy density as that of batteries [1, 2]. Supercapacitors are usually categorized into two different types according to their different charge storage processes, one is the electric double-layer capacitor (EDLC) and the other one is the pseudo-capacitor [3]. In the past, various types of carbon materials have been used as electrode materials for EDLCs, such as activated carbon [4], carbon black [5], mesoporous carbon [6], carbon nanotubes [7], graphite [8] and graphene [9, 10]. And a variety of metal

Address correspondence to E-mail: xzhao@dhu.edu.cn; qhzhang@dhu.edu.cn

oxides, metal nitrides and conductive polymers, such as manganese dioxide [11, 12], copper oxide [13], ruthenium oxide [14], Stannic oxide [15], Molybdenum dioxide [16], titanium dioxide [17], titanium nitride [18], polyaniline [19], polypyrrole [20] and polyethylenedioxy thiophene [21], have been widely used for the fabrication of pseudocapacitors via reversible faradaic reactions to store charges.

With the development of new technologies, one-dimensional flexible electronics are more in need in the future, and the demand for one-dimensional electrodes faces rapid growth. The topic has propelled researchers and companies to invent and fabricate new one-dimensional electrodes to fill the requisition of the electric devices. Firstly, metallic fibers have been traditionally used because of the advantages of high conductivity and availability, but their tendency to oxidize under humid conditions and their heavy weight limit their use in one-dimensional electronics [22]. Carbon fibers are well known not only for their high conductivity and high mechanical strength but also for their low density and inertness under ambient conditions, as well as their ability to be easily woven into fabrics, which make them attractive as one-dimensional electrode materials for various energy storage devices [23]. Until now, electrodes based on carbon fibers have mostly adopted a core–shell structure or engaging layers on the surface of carbon fibers, which may easily falloff of the carbon fibers. This is usually caused by weak contact with the core or a lack of strong molecular interactions between layers, as well as volume changes during the charge–discharge process of the electrode. Another shortage that prevents actual applications of carbon fibers is that they traditionally rely on the storage of charge in the electric double layer, which usually cannot provide a large specific capacitance.

Herein, we adopted a facile method to make layers directly from the surface of carbon fibers. Because the layers were formed directly from the carbon fibers, there is a strong interconnection between the layers and the carbon fibers to avoid unwanted flaking from the main body during the electrochemical reaction process or under external forces when materials fabricated using the electrodes are actually used. An adjusted Hummers' method was used to make oxidized graphite layers on the surface of carbon fibers, containing oxygen functional groups that could provide a pseudocapacitance, which could largely improve the specific capacitance of the carbon fiber electrodes.

Experimental section

Materials

All of the reagents were purchased from Sinopharm Chemical Reagents Co., Ltd. and used as received. Carbon fibers were purchased from Zhongfu-Shenying Carbon Fiber Co., Ltd.

Electrode preparation

A bundle of carbon fibers (CFs) was immersed in concentrated sulfuric acid (H_2SO_4) at room temperature for 2 h, and then three-times washed using deionized water and dried at 60 °C in the oven for 12 h. Processed CFs (0.5 g) were immersed in 20 mL of H_2SO_4 with slowly stirring. Then, 10 mL of nitric acid (HNO_3) was added. The container was placed in an ice bath for 1 h, and 3 g of potassium permanganate ($KMnO_4$) was slowly added. Afterward, the temperature of the container was set to 35 °C for 3 h, and 100 mL of deionized (DI) water was slowly added. After 3 h, hydrogen peroxide (H_2O_2) was slowly added until no gas bubbles evolved, and the solution became transparent. The CFs were dried in an oven at 60 °C for 12 h after five-times cleaning with DI water. The resultant oxidized CFs were designated as CF-O.

The CFs (100 mg) were uniformly distributed in the bottom of a Teflon beaker. The thickness of a covering of CFs was very thin so the bottom of the beaker was even almost seen. And put the beaker in the middle of the pallet and processed in a microwave using low power (the rated power of the microwave was 700 W) for different durations. The samples after being treated by the microwave were designated as CF-X (X = 1, 2, 4, 6, 8, and 10 min).

CF-6 (100 mg) was reduced in a 50-mL hydrothermal reaction vessel with 0.5 mL hydrazine hydrate at 80 °C for 15 h. During the reduction progress, the vessel was sealed and opened in fume hood when it cooled down. Then, the resulting sample was dried in an oven at 60 °C for 1 h after five-times cleaning with DI water (designated as CF-R).

Characterization

Field-emission scanning electron microscopy (FESEM) was performed using a Hitachi S-4800. Fourier transform infrared spectroscopy (FTIR) was performed with a Thermo Nicolet 6700 from 4000 to 400 cm^{-1}, and Laser Raman spectrometry was carried out on a Renishaw inVia Reflex with He-Ne laser excitation at 633 nm from 150 to 3200 cm^{-1}. The elemental analysis utilized the elemental analyzer VarioEI III. The X-ray photoelectron spectroscopy (XPS) analysis was conducted with a 5000 C ESCA System (Mg Kαhν = 1253.6 eV) to characterize the chemical state of the samples.

Cyclic voltammetry (CV), galvanostatic charge–discharge curves and electrochemical impedance spectroscopy measurements were conducted using a PGSTAT302 N AutoLab electrochemical workstation. Cycling stability measurements used a LANHE CT2001A testing device. The electrochemical measurements of the samples were carried out in a three-electrode electrochemical cell containing 1.0 mol dm^{-3} H_2SO_4 aqueous solution as the electrolyte, a platinum gauze counter electrode, and a saturated calomel electrode as the reference electrode at room temperature. A two-electrode configuration was fabricated with two electrodes in parallel and a 1 M H_2SO_4 aqueous solution as the electrolyte.

The specific capacitance of a single electrode in the three-electrode configuration was calculated from the charge–discharge curves using the following equation:

$$C_{electrode} = \frac{I \cdot \Delta t}{m_{electrode} \cdot \Delta V} \tag{1}$$

where I is the discharge current (A), $m_{electrode}$ is the mass of the electrode (g), v is the scan rate (V s^{-1}), ΔV is the potential window (V), and Δt is the discharge time(s).

The specific capacitance of the two-electrode supercapacitors (SCs) was determined from their charge–discharge curves by the following equation:

$$C_{cell} = \frac{I\Delta t}{m_{cell}\Delta V} \tag{2}$$

where I is the discharge current (A), m_{cell} is the mass of the two electrodes (g), v is the scan rate (V s^{-1}), ΔV is the potential window (V), and Δt is the discharge time (s).

The volumetric energy density (E_v) and power density (P_v) of the cell were calculated by the following equations:

$$E_v = \frac{1}{2}C_{v,cell}\Delta V^2 \tag{3}$$

$$P_v = \frac{E_v}{\Delta t} \tag{4}$$

where ΔV is the potential window (V), Δt is the discharge time (s), $C_{v,cell}$ is the volumetric capacitance of the device (F cm^{-3}), E_V is the volumetric energy density (mWh cm^{-3}) of the device, and P_V is the volumetric power density (w cm^{-3}) of the device.

The densities of each electrode and each device were measured by a densitometer (Quantachrome, Ultrapycnometer 1000), and then the volume ($V_{electrode}$ or V_{cell}) was obtained by dividing the mass by the density.

Results and discussion

The fabrication process of the reduced CFs via microwave treatment is illustrated in the scheme (Fig. 1). A commercially available CF bundle, with an individual fiber diameter of ~ 7 μm, was oxidized using a revised Hummers' method with concentrated H_2SO_4, concentrated HNO_3 and $KMnO_4$ after being washed by a 10 M H_2SO_4 solution and DI water at room temperature. Then, the oxidized CFs (designated as CF-O) were processed using a microwave for different times while uniformly laid under the bottom of a Teflon beaker. The resultant CFs were marked as CF-X (X denoting the processing time). To obtain reduced CFs (designated as CF-R), hydrazine hydrate was used to process the microwave-treated CFs in hydrothermal reaction vessel at 80 °C for 15 h.

The FESEM image (Fig. 2a) shows that the surfaces of the original CFs were smooth, and after oxidation (Fig. 2b), the surface became rough and some pores with diameters of dozens of nanometers appeared on them. Then, after the microwave processing, the surface of the CFs became rougher, and more pores were distributed uniformly on the surface, which was covered by the resultant oxidized graphite layers (Fig. 2c). With increasing microwave processing time, significantly more pores appeared on the CF surface. When the processing time reached 10 min, the overextended duration of microwave treatment resulted in the exfoliation of graphite layers from the

Figure 1 Schematic illustration of the fabrication of oxidized, microwave-treated and reduced carbon fibers.
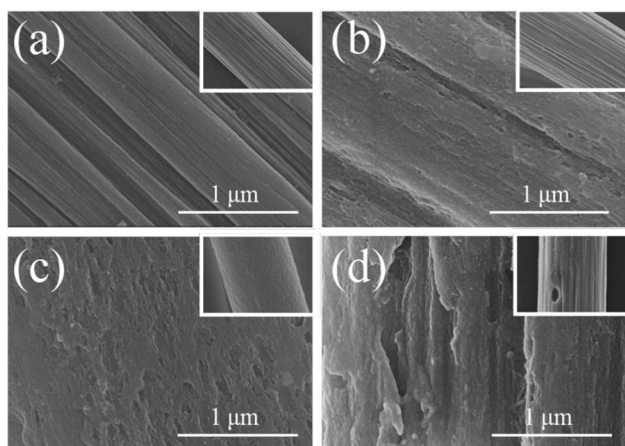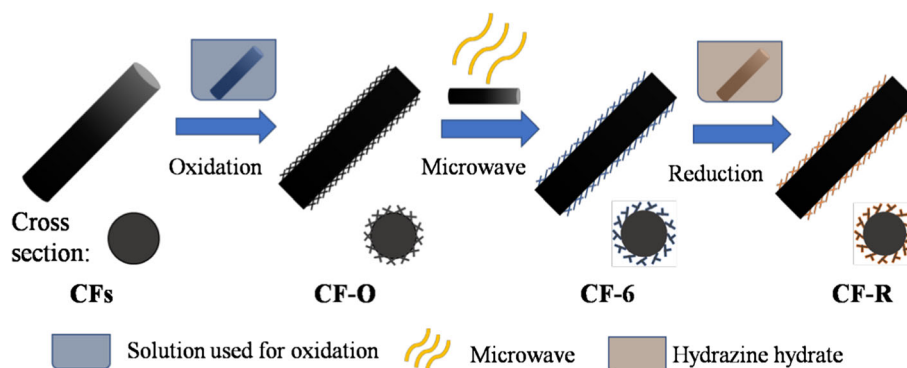

Figure 2 SEM images of **a** the original CFs, **b** CFs after oxidation, **c** CF-6 with microwave processing and **d** CF-R after reduction.

CF surface (Figure S1). However, there were still nanosized pores distributed uniformly on the bare surface (Figure S1e and S1f). With the reduction by hydrazine hydrate, the structure of the CF surface was well maintained with the pores and graphite layers distributed uniformly (Fig. 2d).

The FTIR spectrum (Fig. 3a) exhibited a band at 3433 cm^{-1} and shoulder band at 3258 cm^{-1} corresponding to the stretching vibrations of structural OH groups and physisorbed water molecules because the oxygen functional groups on the CF surface were strongly affected by humidity. The small band at 1733 cm^{-1} has often been related to the C=O stretching of COOH groups situated at the edges of graphite, while the peaks near 1258 and 1054 cm^{-1} were assigned to the C–O stretching vibration and C–OH stretching vibration, respectively [24]. All of the above proved that carboxyl and hydroxyl groups were formed on the CF surfaces. A relatively strong band situated near 1100 cm^{-1} indicated the stretching vibration of C–O–C. The two strong peaks at 2923 and 2854 cm^{-1} were related to the CH_2 symmetric and antisymmetric stretching vibrations. A quantum chemical study of model carbon compounds showed OH groups, via cooperative effects, induced ring vibrations near 1630 cm^{-1} and an IR absorption in the $1420–1480 \text{ cm}^{-1}$ range [25]. For the peak at 1258 cm^{-1}, after oxidation, its relative intensity increased, which means more C–O bonds are formed. For the sample from CF-1 to CF-10, its

Figure 3 **a** FTIR spectra of CFs, oxidized CFs, microwaved CFs and reduced CFs. **b** Raman spectra of CFs, oxidized CFs, microwaved CFs and reduced CFs.
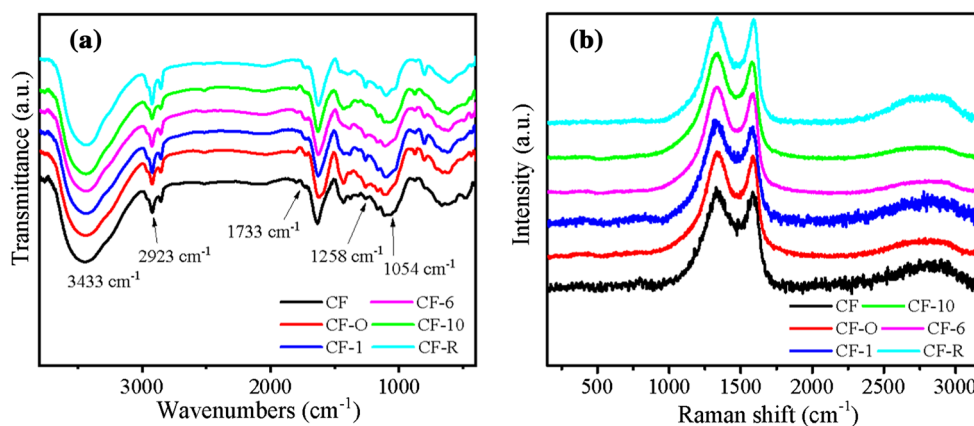
relative intensity decreased. Because with much more microwave processing time, parts of oxygen functional groups could be consumed, and oxidized graphite layers will be exfoliated and detached from the CFs. For CF-R, the C–N bonds those formed during the reduction progress may contribute for the relative increase in the intensity at 1258 cm^{-1}.

The pair of bands at 1330 and 1580 cm^{-1} in the Raman spectrum are the most diagnostic features and are designated as the D band and G band (Fig. 3b). The D band accounts for the presence of defects, and the G band represents the graphitic order [26]. The band at approximately 2750 cm^{-1} is characteristic of crystalline CFs, although its detailed appearance is affected by the presence of disorder [27]. The D/G intensity ratio (I_D/I_G) has been widely used for the relationship between both band intensities, which should be proportional to the degree of structural order with respect to the graphitic structure [28]. The values of I_D/I_G showed no significant fluctuations, which indicated that the oxidation, microwave treatment and reduction induced no additional defects to the original structure (Table S1).

From the elemental analysis, the oxygen content increased significantly for CF-O, which was nearly twelve times more than that of the original CFs, while the nitrogen content slightly decreased (approximately 1.4%, Fig. 4). The process and results contained within are nearly the same as those obtained for the preparation of oxidized graphene using Hummers' method. With increasing microwave time, the oxygen content exhibited a slightly decreasing trend, and the nitrogen content trend was the opposite. The number of surface graphite layers that exfoliated and detached from the CF-O increased

with microwave processing time, which was also proved by the SEM images (Figure S1). After the reduction using hydrazine hydrate, the oxygen content apparently decreased to 12.9%, which was nearly half of that of CF-O and the microwave-treated CFs; while CF-R had a nitrogen content of 7.5%, which increased twofold compared with the sample processed with oxidation and treated with microwave irradiation.

The compositions of the CF surfaces were also investigated by XPS. The survey scans clearly showed that N 1 s and O 1 s peaks existed on the surface of CF-R (Fig. 5a), while those for CF, CF-O and CF-6 showed the N 1 s peaks were insignificant (Figure S2). From the narrow scans for CF-R, the peak at 285.6 eV belonged to C–N, while the other four peaks at 284.73, 286.9, 288.32, 289.98 eV were assigned to the carbon atoms of C–C, C–O, C=O, COOH functional groups, respectively (Fig. 5b) [29]. The assignments were the same for the CFs, CF-O and CF-6 (Figure S2). The N 1 s narrow scan showed that pyridinic N (C=N–C), pyrrolic N (H–N–(C)$_2$), graphitic N (N–(C)$_3$) and graphitic N–O existed on the surface of CF-R, corresponding to the peaks at 399.24, 399.92, 401.16, 402.2 eV, respectively (Fig. 5c) [30]. The elemental contents derived from XPS had the same trend as the results of elemental analysis (Table S2). After oxidation, there was an increase in the C content, and the N contents had a significant increase after the reduction (Fig. 5d).

The specific capacitances of the obtained samples were firstly evaluated with the three-electrode system by cyclic voltammetry (CV) in the voltage range of 0–0.8 V (Fig. 6). The area derived from the CV curve for the CFs was significantly smaller than those of
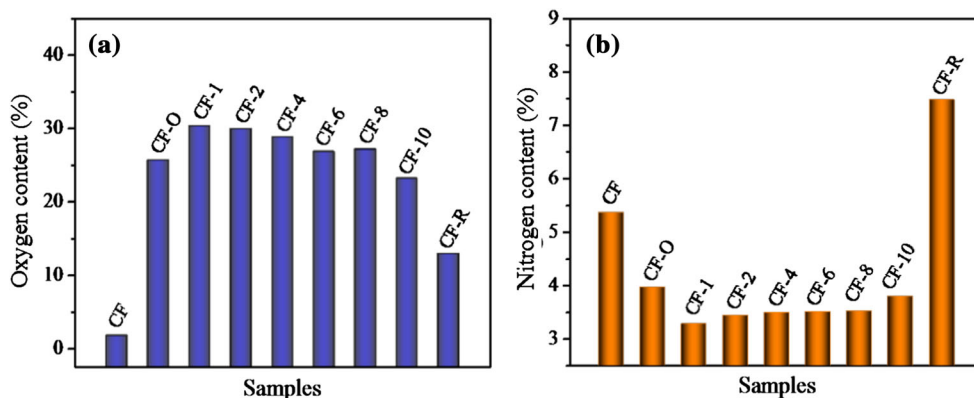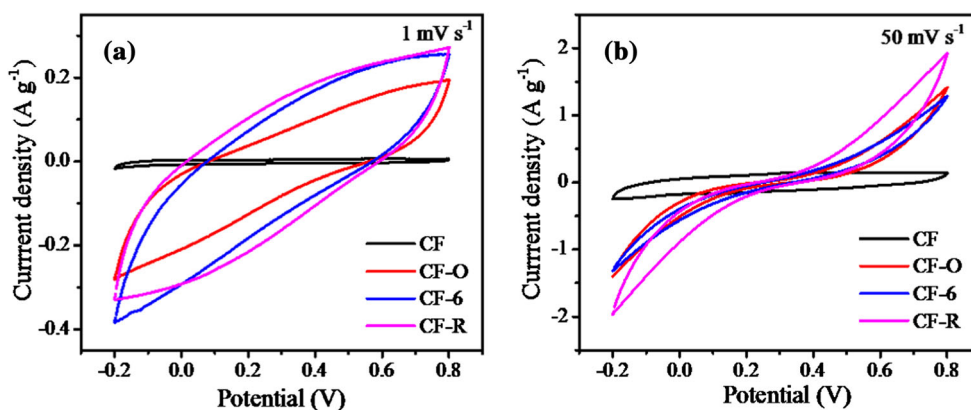

Figure 4 **a** Oxygen and **b** nitrogen contents of different samples.

Figure 5 **a** Wide XPS scan of CF-R; the C 1 s (**b**) and N 1 s (**c**) XPS spectra of CF-R; **d** the elemental contents of different samples derived from XPS.
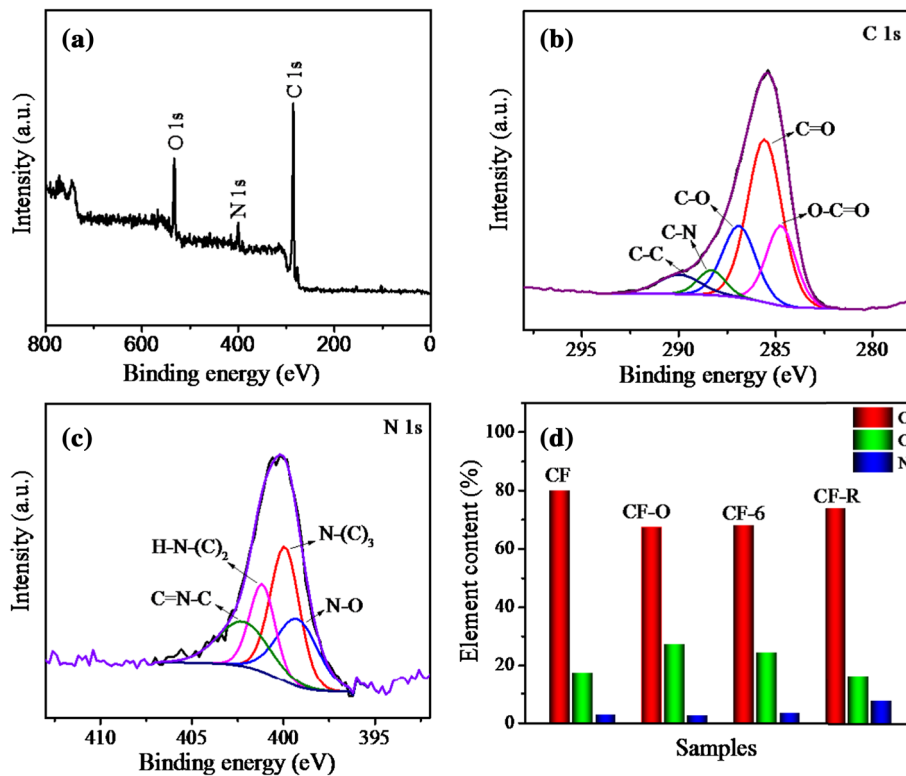
Figure 6 CV curves of different samples collected at **a** 1 mV s^{-1} and **b** 50 mV s^{-1}.

CF-O, CF-6, CF-R at a scan rate of 1 mV s^{-1} (Fig. 6a), indicating an improvement in the specific capacitance after oxidization, microwave and reduction treatments. It is said that in an acidic aqueous electrolyte, the electrons on oxygen functional groups attract H_3O^+, which leads to the separation of the positive and negative charges, thus, facilitating the redox reaction. Especially, for hydroxyl and quinone, this can provide a substantially higher pseudocapacitance than that provided by other oxygen functional groups [31, 32]. The CV curves of CF-O, CF-6, and CF-R exhibited symmetric characteristics at the axis of zero current and approached the quasi-rectangular shape over a full scan range at 1 mV s^{-1}, which indicated that those samples had a typical capacitive behavior [33]. The reason for the capacitance increase in CF-6 compared with that of CF-O may be the result of increased spacing between the graphite layers caused by the microwave exfoliation. Furthermore, more pores inside the graphite layers facilitated the migration of the electrolyte, which could promote an increase in the capacitance. At a scan rate of 50 mV s^{-1}, the CV curves of CF-O, CF-6 and CF-R changed, exhibiting a different shape from those at the scan rate of 1 mV s^{-1}, indicating a resistance caused by the oxygen functional groups existed,

while the CV profiles of the CFs without oxidized graphite layers on the surface could maintain a nearly rectangular shape at a scan rate of 50 mV s^{-1} (Fig. 6b). This showed that the functional contained groups had a great effect on the electron transport at a high scan rate.

The galvanostatic charge–discharge curves showed the same results as the CV curves. The CR-R and CR-6 had nearly the same specific capacitances, which were 213.3 and 218.9 F g^{-1}, respectively; both were nearly twice as much as that of CF-O and forty times more than that of the CFs, again indicating the contribution of the surface oxygen functional groups (Fig. 7a, b). The results also showed that N-doping could make up for the loss of capacitance from the decrease in oxygen functional groups, which was confirmed by the elemental analysis [34, 35]. The best microwave processing time was 6 min, which was confirmed by galvanostatic charge–discharge curves at a current density of 0.1 A g^{-1} (Figure S3). The trend in capacitance change proved that the disorder degree of oxidized graphite layers increased with the microwave processing time within 6 min, while longer than 6 min exfoliated the oxidized graphite layers from the CF main body (Fig. 7b). The electrochemical performance of the CFs that was directly

processed with microwave without oxidation has also been studied (Figure S4). The discharge time of it was almost the same with that of CFs when tested at the current density of 0.1 A g^{-1}.

The calculated IR drops showed that there was a big change in the resistance of all the samples (Inset of Fig. 7a). After oxidization, the IR drop for CF-O increased to 0.28 V from 0.02 V of CF, which indicated an abundance of oxygen functional groups formed on the surface of the CFs. There were little effects on the IR drop from the microwave treatment when the period of processing was less than 6 min. However, after 6 min, the IR drop had a slight drop corresponding to the CF microwave process shown in the SEM images (Figure S1). EIS measurements were also conducted to show the charge transfer resistance of the samples (Fig. 7c). Compared with the CFs, the EIS plots of CF-O, CF-6, and CF-R all had a large semicircle at the lower frequency region, which was probably from the slow electron transfer caused by the electrochemical reaction of the oxygen functional groups. The equivalent simulation circuits also confirmed that a charge transfer process consisted of two steps through two electrical parts connected in series (Figure S5), and the equivalent series resistances showed the same trend with those of the resistances

Figure 7 **a** Charge–discharge curves of various samples with the inset of the IR drop for those with different microwave processing times; **b** specific capacitances of different samples at 0.1 A g^{-1}; **c** Nyquist plots of various samples with the inset showing the enlarged profiles; **d** the curve of cycling life for CF-R at a current density of 0.2 A g^{-1}.
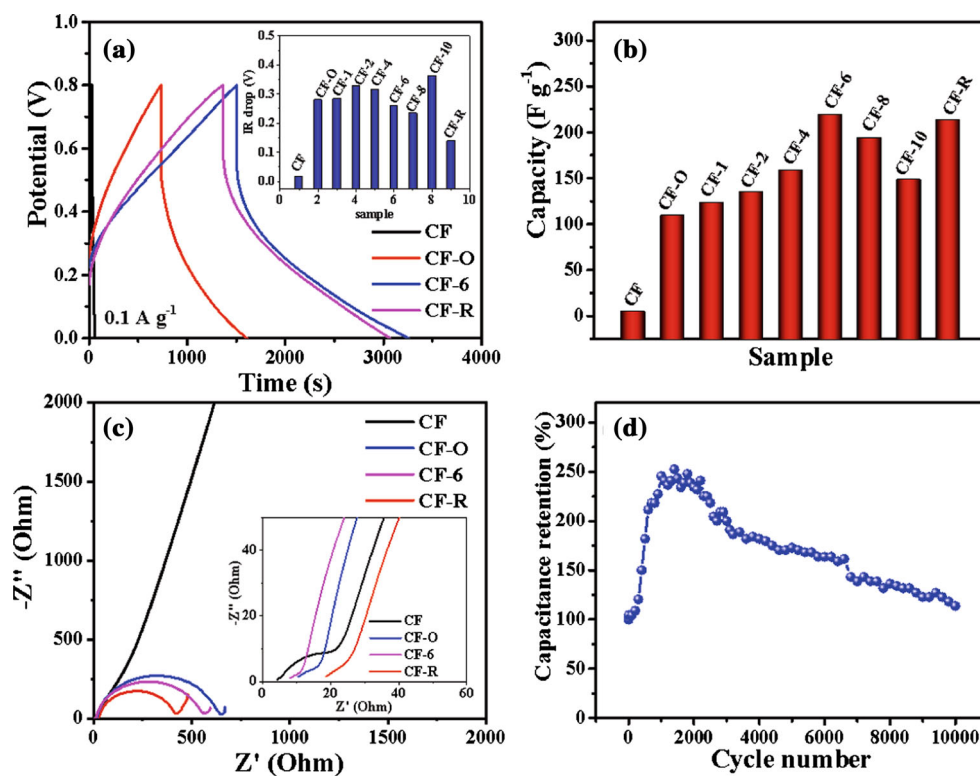
calculated from the galvanostatic charge–discharge curves (Table S3). The resistance of a bundle of fibers with the length of 1.5 cm has also been performed (Table S4). The results proved it again that CF-R has a better conductivity than that of CF-O and CF-6. From the specific capacitances derived from the simulation, the electrodes based on CF-O, CF-6, and CF-R had smaller double-layer capacitances than those of the electrodes made of the CFs, which indicated the surfaces of the oxidized CFs consisted of multiple graphite layers with an abundance of oxygen functional groups on them. Meanwhile, there was little bare carbon surface remaining to provide double-layer capacitance [36, 37]. The influence of oxygen functional groups was greater than that of the specific surface area of carbon materials [38]. From the Bode plots, CF-O, CF-6, and CF-R reached high resistance plateaus at 3 Hz, while the CFs only had a smaller resistance, which revealed that large resistances existed for CF-O, CF-6, and CF-R on the surface (Figure S5). This result was caused by the abundant oxygen functional groups. From the phase plots, CF-O, CF-6, and CF-R each had a symmetric phase angle peak, meaning a semicircle in the Nyquist plots, while the CFs only had a half-angle phase peak, meaning a quarter-circle (Figure S5). All of this showed that CF-O, CF-6, and CF-R had a slow charge transfer process, caused by the surface oxygen functional groups, compared with that of the CFs.

The cycling test showed that the electrode made of CF-R had a good durability, and the specific capacitance retention was 113.6% after 10000 cycles (Fig. 7d). Before 2000 cycles, an increasing trend developed and then declined. It is said that the wettability of carbon materials can be improved by oxygen functional groups, which are helpful for enhancing the ion diffusion in an aqueous electrolyte [39, 40]. Additionally, the reason for the decrease is that the oxidation/reduction processes of the oxygen functional groups are quasi-reversible processes [41].

To further evaluate the practical applications of the as-prepared samples, two electrodes were used in parallel to fabricate a symmetric supercapacitor with a 1 M H_2SO_4 aqueous solution as the electrolyte. The CV curves of devices with CF-O, CF-6, and CF-R were nearly rectangular in shape, indicating the good capacitive behavior of all the electrodes at a scan rate of 1 mV s^{-1} (Fig. 8a). The areas under the CV curves of CF-R and CF-6 were larger than that of CF-O, which was consistent with the results from the three-electrode configuration measurements. Although there was little change in the CV curves for the symmetric supercapacitors from the quasi-rectangular shape at a scan rate of 50 mV s^{-1}, they were even closer to a rectangle than those of the electrodes tested in the three-electrode configuration (Fig. 8b). In addition, at high scan rates, the electrical double-layer capacitance would dominate the capacitive performance, while a few oxygen functional groups from the outside graphite layers continued to contribute to the capacitance, which was responsible for the tilt to the quasi-rectangular shape.

The galvanostatic charge–discharge curves showed the same results as those using the three-electrode configuration (Fig. 8c). The specific capacitances of symmetric supercapacitors fabricated using CF-6 and CF-R were 30.3 and 29.2 F g^{-1}, respectively. Both were larger than that of the symmetric supercapacitor made of CF-O. Furthermore, the IR drop of the CF-R supercapacitor was 0.18 V, smaller than those of the CF-O and CF-6 supercapacitors (0.26 V and 0.31 V, respectively), which again confirmed that the reduction using hydrazine hydrate was effective in removing parts of the electrode surface oxygen functional groups to improve the conductivity, while maintaining the high specific capacitance by N-doping. The semicircle in the Nyquist plots also showed the symmetric supercapacitor using CF-R as the electrodes had a smaller charge transfer resistance than those of the devices made of CF-O and the CFs, which also was proved by the equivalent series resistance diagrams (Figs. 8d and S6). The charge transfer process contained two steps including a fast electron transportation caused by the electrical double layers and a slow one caused by the electrochemical reaction of the oxygen functional groups on the outside graphite layer of the electrodes. The cycling durability of the assembled device was good, and 57.8% of the specific capacitance remained after 10000 cycles (Fig. 8e). The specific capacitance of the supercapacitor made from CF-R in this study compares favorably with other studies in terms of energy and power densities (Fig. 8f). The Ragone plots show that the device exhibited volumetric energy densities of 3.22 mWh cm^{-3} (80 mW cm^{-3}) and 6.50 mWh cm^{-3} (40 mW cm^{-3}) at current densities of 0.1 and 0.05 A g^{-1}, respectively, which revealed good energy densities when tested at low current densities [42–49].

Figure 8 CV curves of symmetric supercapacitors at scan rates of **a** 1 mV s-1 and **b** 50 mV s-1; **c** charge–discharge curves of different samples at a current density of 0.1 A g-1; **d** Nyquist plots of CF-O, CF-6, and CF-R symmetric supercapacitors; **e** the cycling life of the supercapacitor based on CF-R at a current density of 0.1 A g-1; **f** Ragone plots of the assembled device compared with reported results.
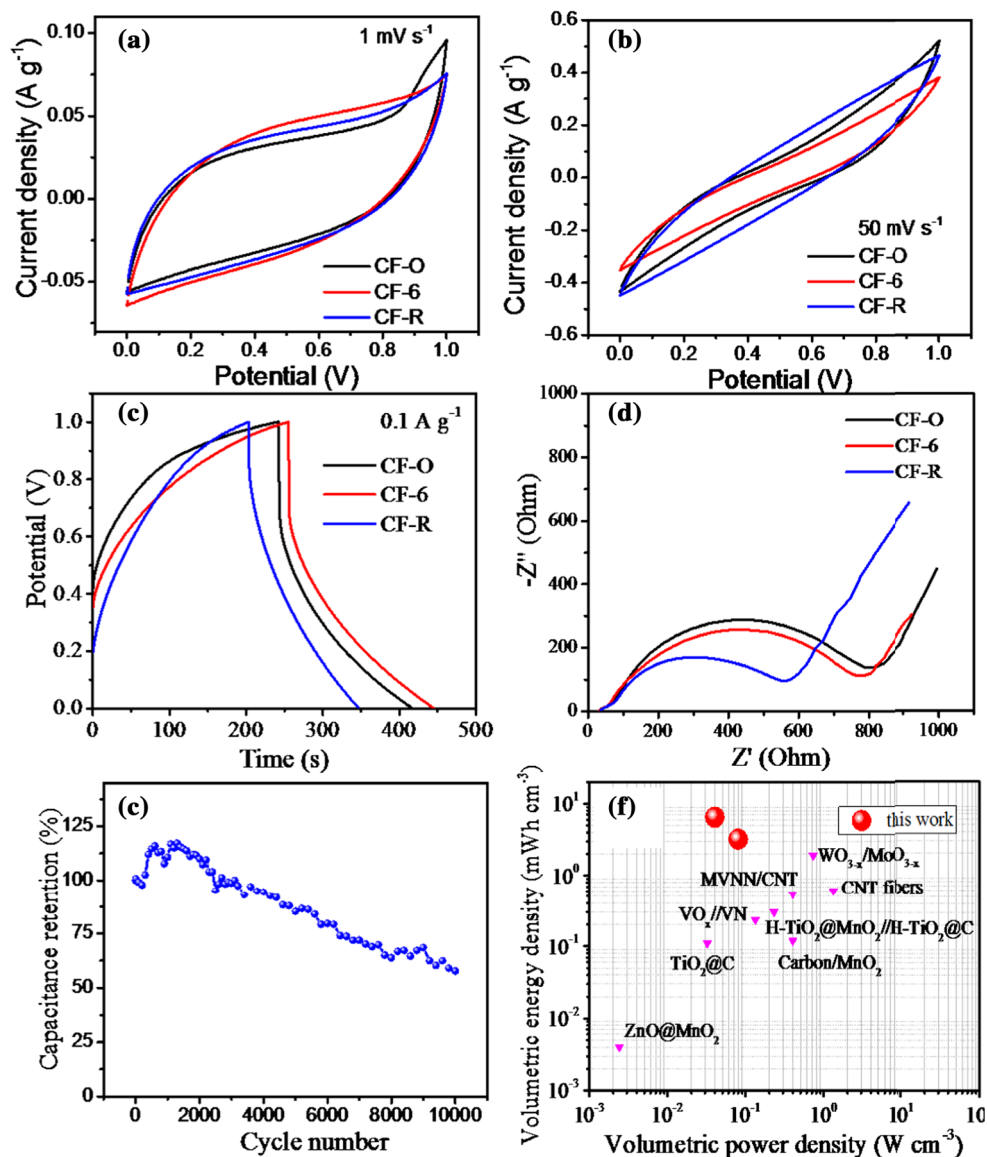
Conclusions

In conclusion, a facile method was used to fabricate one-dimensional and high electrochemical performance electrodes based on CFs with oxidized graphite layers and subsequently reduced by hydrazine hydrate. The core of the CFs provided good conductivity as the underlying material, while the oxidized graphite layers, endowed with a large number of oxygen functional groups, greatly contributed to the pseudocapacitance of the electrodes, which was accounted for by the good electrochemical performance. The resultant CF-R electrode reached 213.3 F g^{-1}, forty times greater than that of pure CFs at a current density of 0.1 A g^{-1}. The electrodes also showed outstanding cycling stability (nearly 100% retention after 1000 cycles). The symmetric supercapacitors based on CF-R also showed high energy densities of 3.22 mWh cm^{-3} (80 mW cm^{-3}) and 6.50 mWh cm^{-3} (40 mW cm^{-3}) at current densities of 0.1 and 0.05 A g^{-1}, respectively. Although the conductivity remains to be improved, this strategy

provides direction for the design of large-scale one-dimensional electrodes with good specific capacitance for future energy storage systems.

Acknowledgements

Compliance with ethical standards

Conflict of interest The authors declare that they have no conflict of interest.

Electronic supplementary material: The online version of this article (https://doi.org/10.1007/s10853-018-2366-5) contains supplementary material, which is available to authorized users.

References

[1] Simon P, Gogotsi Y (2008) Materials for electrochemical capacitors. Nat Mater 7(11):845–854

[2] Zhang LL, Zhao XS (2009) Carbon-based materials as supercapacitor electrodes. Chem Soc Rev 38(9):2520–2531

[3] Wang G, Zhang L, Zhang J (2012) A review of electrode materials for electrochemical supercapacitors. Chem Soc Rev 41(2):797–828

[4] Denisa H-J, Seredych M, Lu GQ, Bandosz TJ (2009) Combined effect of nitrogen- and oxygen-containing functional groups of microporous activated carbon on its electrochemical performance in supercapacitors. Adv Funct Mater 19(3):438–447

[5] Kossyrev P (2012) Carbon black supercapacitors employing thin electrodes. J Power Sources 201:347–352

[6] Kang D, Liu Q, Gu J, Su Y, Zhang W, Zhang D (2015) "Egg-Box"-assisted fabrication of porous carbon with small mesopores for high-rate electric double layer capacitors. ACS Nano 9(11):11225–11233

[7] Xu P, Gu TL, Cao ZY, Wei BQ, Yu JQ, Li FX, Byun JH, Lu WB, Li Q, Chou TW (2014) Carbon nanotube fiber based stretchable wire-shaped supercapacitors. Adv Energy Mater 4(3):1–7

[8] Ji J, Liu J, Lai L, Zhao X, Zhen Y, Lin J, Zhu Y, Ji H, Zhang LL, Ruoff RS (2015) In situ activation of nitrogen-doped graphene anchored on graphite foam for a high-capacity anode. ACS Nano 9(8):8609–8616

[9] Ji J, Li Y, Peng W, Zhang G, Zhang F, Fan X (2015) Advanced graphene-based binder-free electrodes for high-performance energy storage. Adv Mater 27(36):5264–5279

[10] Wang Y, Yu F, Zhu M, Ma C, Zhao D, Wang C, Zhou A, Dai B, Ji J, Guo X (2018) N-Doping of plasma exfoliated graphene oxide via dielectric barrier discharge plasma treatment for the oxygen reduction reaction. J Mater Chem A 6(5):2011–2017

[11] Zhang J, Zhao X, Huang Z, Xu T, Zhang Q (2016) High-performance all-solid-state flexible supercapacitors based on manganese dioxide/carbon fibers. Carbon 107:844–851

[12] Zhu S, Li L, Liu J, Wang H, Wang T, Zhang Y, Zhang L, Ruoff RS, Dong F (2018) Structural directed growth of ultrathin parallel birnessite on β-MnO$_2$ for high-performance asymmetric supercapacitors. ACS Nano 12(2):1033–1042

[13] Bae J, Song MK, Park YJ, Kim JM, Liu M, Wang ZL (2011) Fiber supercapacitors made of nanowire-fiber hybrid structures for wearable/flexible energy storage. Angew Chem Int Ed 50(7):1683–1687

[14] Arabale G, Wagh D, Kulkarni M, Mulla IS, Vernekar SP, Vijayamohanan K, Rao AM (2003) Enhanced supercapacitance of multiwalled carbon nanotubes functionalized with ruthenium oxide. Chem Phys Lett 376(1–2):207–213

[15] Liang J, Yuan C, Li H, Fan K, Wei Z, Sun H, Ma J (2018) Growth of SnO$_2$ nanoflowers on N-doped carbon nanofibers as anode for Li- and Na-ion batteries. Nano-Micro Lett 10(2):21

[16] Liang J, Gao X, Guo J, Chen C, Fan K, Ma J (2018) Electrospun MoO$_2$@NC nanofibers with excellent Li$^+$/Na$^+$ storage for dual applications. Sci China Mater 61(1):30–38

[17] Deng X, Wei Z, Cui C, Liu Q, Wang C, Ma J (2018) Oxygen-deficient anatase TiO$_2$@C nanospindles with pseudocapacitive contribution for enhancing lithium storage. J Mater Chem A 6(9):4013–4022

[18] Xie Y, Xia C, Du H, Wang W (2015) Enhanced electrochemical performance of polyaniline/carbon/titanium nitride nanowire array for flexible supercapacitor. J Power Sources 286:561–570

[19] Zhang K, Zhang LL, Zhao XS, Wu J (2010) Graphene/polyaniline nanofiber composites as supercapacitor electrodes. Chem Mater 22(4):1392–1401

[20] Mini PA, Balakrishnan A, Nair SV, Subramanian KRV (2011) Highly super capacitive electrodes made of graphene/poly(pyrrole). Chem Commun 47(20):5753–5755

[21] Laforgue A (2011) All-textile flexible supercapacitors using electrospun poly(3,4-ethylenedioxythiophene) nanofibers. J Power Sources 196(1):559–564

[22] Nam S, Jang J, J-j Park, Kim SW, Park CE, Kim JM (2012) High-performance low-voltage organic field-effect

transistors prepared on electro-polished aluminum wires. ACS Appl Mat Interfaces 4(1):6–10

[23] Liu XY, Zhou M, Chen C, Zhang YX (2017) Electrochemical capacitor performance of TiO$_2$ nanostructures and porous MnO$_2$ composite supported on carbon fiber paper. Ceram Int 43(13):10595–10600

[24] Szabó T, Berkesi O, Forgó P, Josepovits K, Sanakis Y, Petridis D, Dékány I (2006) Evolution of surface functional groups in a series of progressively oxidized graphite oxides. Chem Mater 18(11):2740–2749

[25] Fuente E, Menéndez JA, Díez MA, Suárez D, Montes-Morán MA (2003) Infrared spectroscopy of carbon materials: a quantum chemical study of model. J Phys Chem B 107(26):6350–6359

[26] Kudin KN, Ozbas B, Schniepp HC, Prud'homme RK, Aksay IA, Car R (2008) Raman spectra of graphite oxide and functionalized graphene sheets. Nano Lett 8(1):36–41

[27] Galiotis C, Batchelder DN (1998) Strain dependences of the first- and second-order Raman spectra of carbon fibres. J Mater Sci Lett 7:545–547

[28] Lespade P, Marchand A, Couzi M, Cruege F (1984) Caracterisation de materiaux carbones par microspectrometrie Raman. Carbon 22(4/5):375–385

[29] Jeong H-K, Lee YP, Lahaye RJWE, Park M-H, An KH, Kim IJ, Yang C-W, Park CY, Ruoff RS, Lee YH (2008) Evidence of graphitic AB stacking order of graphite oxides. J Am Chem Soc 130(4):1362–1366

[30] Artyushkova K, Kiefer B, Halevi B, Knop-Gericke A, Schloglc R, Atanassov P (2013) Density functional theory calculations of XPS binding energy shift for nitrogen-containing graphene-like structures. Chem Commun 49(25):2539–2541

[31] Roldán S, Blanco C, Granda M, Menéndez R, Santamaría R (2011) Towards a further generation of high-energy carbon-based capacitors by using redox-active electrolytes. Angew Chem 50(7):1699–1701

[32] Singh C, Paul A (2015) Physisorbed hydroquinone on activated charcoal as a supercapacitor: an application of proton-coupled electron transfer. J Phys Chem C 119(21):11382–11390

[33] Lu X, Liu T, Zhai T, Wang G, Yu M, Xie S, Ling Y, Liang C, Tong Y, Li Y (2014) Improving the cycling stability of metal-nitride supercapacitor electrodes with a thin carbon shell. Adv Energy Mater 4(4):1300994

[34] Kim DJ, Kim JK, Lee JH, Cho HH, Bae Y-S, Kim JH (2016) Scalable and bendable organized mesoporous TiN films templated by using a dual-functional amphiphilic graft copolymer for solid supercapacitors. J Mater Chem A 4(32):12497–12503

[35] Ramanuja N, Levy RA, Dharmadhikari SN, Ramos E, Pearce CW, Menasian SC, Schamberger PC, Collins CC (2002) Synthesis and characterization of low pressure chemically vapor deposited titanium nitride films using TiCl$_4$ and NH$_3$. Mater Lett 57(2):261–269

[36] Chmiola J, Largeot C, Taberna P-L, Simon P, Gogotsi Y (2008) Desolvation of ions in subnanometer pores and its effect on capacitance and double-layer theory. Angew Chem 120(18):3440–3443

[37] Largeot C, Portet C, Chmiola J, Taberna P-L, Gogotsi Y, Simon P (2008) Relation between the ion size and pore size for an electric double-layer capacitor. J Am Chem Soc 130(9):2730–2731

[38] Lozano-Castelló D, Cazorla-Amorós D, Linares-Solano A, Shiraishi S, Kurihara H, Oya A (2003) Influence of pore structure and surface chemistry on electric double layer capacitance in non-aqueous electrolyte. Carbon 41(9):1765–1775

[39] Fang B, Binder L (2007) Influence of hydrophobisation of carbon surface on electrochemical capacitor performance. J Electroanal Chem 609(2):99–104

[40] Guo M, Guo J, Jia D, Zhao H, Sun Z, Songa X, Lia Y (2015) Coal derived porous carbon fibers with tunable internal channels for flexible electrodes and organic matter absorption. J Mater Chem A 3(42):21178–21184

[41] Frackowiaka E, Béguinb R (2001) Carbon materials for the electrochemical storage of energy in capacitors. Carbon 39(6):937–950

[42] Xiao X, Li T, Yang P, Gao Y, Jin H, Ni W, Zhan W, Zhang X, Cao Y, Zhong J, Gong L, Yen W-C, Mai W, Chen J, Huo K, Chueh Y-L, Wang Z, Zhou J (2012) Fiber-based all-solid-state flexible supercapacitors for self-powered systems. ACS Nano 6(10):9200–9206

[43] Xiao X, Ding T, Yuan L, Shen Y, Zhong Q, Zhang X, Cao Y, Hu B, Zhai T, Gong L, Chen J, Tong Y, Zhou J, Wang ZL (2012) WO$_{3-x}$/MoO$_{3-x}$ core/shell nanowires on carbon fabric as an anode for all-solid-state asymmetric supercapacitors. Adv Energy Mater 2(11):1328–1332

[44] Xu P, Gu T, Cao Z, Wei B, Yu J, Li F, Byun J-H, Lu W, Li Q, Chou T-W (2014) Carbon nanotube fiber based stretchable wire-shaped supercapacitors. Adv Energy Mater 4(3):1300759

[45] Lu X, Yu M, Wang G, Zhai T, Xie S, Ling Y, Tong Y, Li Y (2013) H-TiO$_2$@MnO$_2$//H-TiO$_2$@C core-shell nanowires for high performance and flexible asymmetric supercapacitors. Adv Mater 25(2):267–272

[46] Xiao X, Peng X, Jin H, Li T, Zhang C, Gao B, Hu B, Huo K, Zhou J (2013) Freestanding mesoporous VN/CNT hybrid electrodes for flexible all-solid-state supercapacitors. Adv Mater 25(36):5091–5097

[47] Yang P, Xiao X, Li Y, Ding Y, Qiang P, Tan X, Mai W, Lin Z, Wu W, Li T, Jin H, Liu P, Zhou J, Wong CP, Wang ZL (2013) Hydrogenated ZnO core-shell nanocables for flexible supercapacitors and self-powered systems. ASC Nano 7(3):2617–2626

[48] Zheng H, Zhai T, Yu M, Xie S, Liang C, Zhao W, Wang SCI, Zhang Z, Lu X (2013) TiO$_2$@C core–shell nanowires for high-performance and flexible solid-state supercapacitors. J Mater Chem C 1(2):225–229

[49] Lu X, Yu M, Zhai T, Wang G, Xie S, Liu T, Liang C, Tong Y, Li Y (2013) High energy density asymmetric quasi-solid-state supercapacitor based on porous vanadium nitride nanowire anode. Nano Lett 13(6):2628–2633